ADVANCED HEALTHCARE MATERIALS
www.advhealthmat.com

Extracellular Trap-Mimicking DNA-Histone Mesostructures Synergistically Activate Dendritic Cells

Priyan D. Weerappuli, Cameron Louttit, Taisuke Kojima, Luke Brennan, Srilakshmi Yalavarthi, Yao Xu, Lukasz J. Ochyl, Midori L. Maeda, Hong Sun Kim, Jason S. Knight, Shuichi Takayama, and James J. Moon**

Extracellular traps (ETs), such as neutrophil extracellular traps, are a physical mesh deployed by immune cells to entrap and constrain pathogens. ETs are immunogenic structures composed of DNA, histones, and an array of variable protein and peptide components. While much attention has been paid to the multifaceted function of these structures, mechanistic studies of ETs remain challenging due to their heterogeneity and complexity. Here, a novel DNA-histone mesostructure (DHM) formed by complexation of DNA and histones into a fibrous mesh is reported. DHMs mirror the DNA-histone structural frame of ETs and offer a facile platform for cell culture studies. It is shown that DHMs are potent activators of dendritic cells and identify both the methylation state of DHMs and physical interaction between dendritic cells and DHMs as key tuning switches for immune stimulation. Overall, the DHM platform provides a new opportunity to study the role of ETs in immune activation and pathophysiology.

Nucleic acids have long been established as immunostimulants, serving as both pathogen-associated molecular patterns (PAMPs) and damage-associated molecular patterns (DAMPs) released during infection and injury, respectively.[1] While previous studies have mainly focused on the immunogenicity of soluble nucleic acids from bacterial, viral, and endogenous sources,[2,3] recent findings have reported the potent immunostimulatory potential of nucleic acids electrostatically complexed to natural or synthetic polycations, including lipids,[4] peptides,[5] and proteins.[6] In a biological corollary of this phenomenon, activated neutrophils and other immune cells have been recently reported to secrete extracellular traps (ETs), decondensed chromatin meshes associated with a diverse assortment of proteins and peptides.[7] Notably, while ETs entrap pathogens and thus limit the spread of infection,[7,8] excessive accumulation of ETs is implicated in overt immune activation[9,10] and pathogenesis of autoimmune disorders including systemic lupus erythematosus.[11–15] Mechanistic studies of this paradoxical phenomenon remain challenging, however, due to the complexity and heterogeneity of ETs; numerous immunostimulatory entities, including nuclear DNA, mitochondrial DNA,[10,16,17] histones,[18] and calprotectin (S100A8/A9),[19,20] are associated with ETs. Additionally, differences in stimuli, disease state, and even neutrophil isolation method yield highly variable ET compositions and therefore impact study reproducibility.[11,19,21] Compounding these problems are the extensive and low-yield procedures required to produce ETs for analysis: it was previously reported that 1×10^6 human peripheral neutrophils yielded only 700–900 ng of ET DNA.[22]

Here, we sought to address these challenges by developing a novel cell-free DNA-histone mesostructure (DHM), a platform composed solely of the two major structural components of ETs: DNA and histones. We show that DHMs mimicking the nanoscale architecture of ETs potently active dendritic cells (DCs) via physical interaction and those DHMs composed of unmethylated DNA further enhance immune activation. These results suggest that classical ET-associated immune activation can be attributed in part to the DNA-histone skeleton of these structures, thus providing novel insight on ET biology.

Specifically, we developed a stepwise sessile droplet-based process for forming DHMs (**Figure 1**A). Our initial studies were focused on identifying the optimal amount of DNA, trehalose, and histone for the formation of stable DHMs

Dr. P. D. Weerappuli, Dr. C. Louttit, L. Brennan, Dr. H. S. Kim, Prof. J. J. Moon
Department of Biomedical Engineering
University of Michigan
2800 Plymouth Drive, Ann Arbor, MI 48109, USA
E-mail: moonjj@umich.edu

Dr. P. D. Weerappuli, Dr. C. Louttit, Y. Xu, Dr. L. J. Ochyl, Prof. J. J. Moon
Biointerfaces Institute
University of Michigan
2800 Plymouth Drive, Ann Arbor, MI 48109, USA

Dr. T. Kojima, M. L. Maeda, Prof. S. Takayama
Wallace H Coulter Department of Biomedical Engineering
Georgia Institute of Technology and Emory University
Atlanta, GA 30332, USA
E-mail: takayama@gatech.edu

S. Yalavarthi, Prof. J. S. Knight
Division of Rheumatology
University of Michigan
Ann Arbor, MI 48109, USA

Y. Xu, Dr. L. J. Ochyl, Prof. J. J. Moon
Department of Pharmaceutical Sciences
University of Michigan
2800 Plymouth Drive, Ann Arbor, MI 48109, USA

The ORCID identification number(s) for the author(s) of this article can be found under https://doi.org/10.1002/adhm.201900926.

DOI: 10.1002/adhm.201900926

 © 2019 WILEY-VCH Verlag GmbH & Co. KGaA, Weinheim

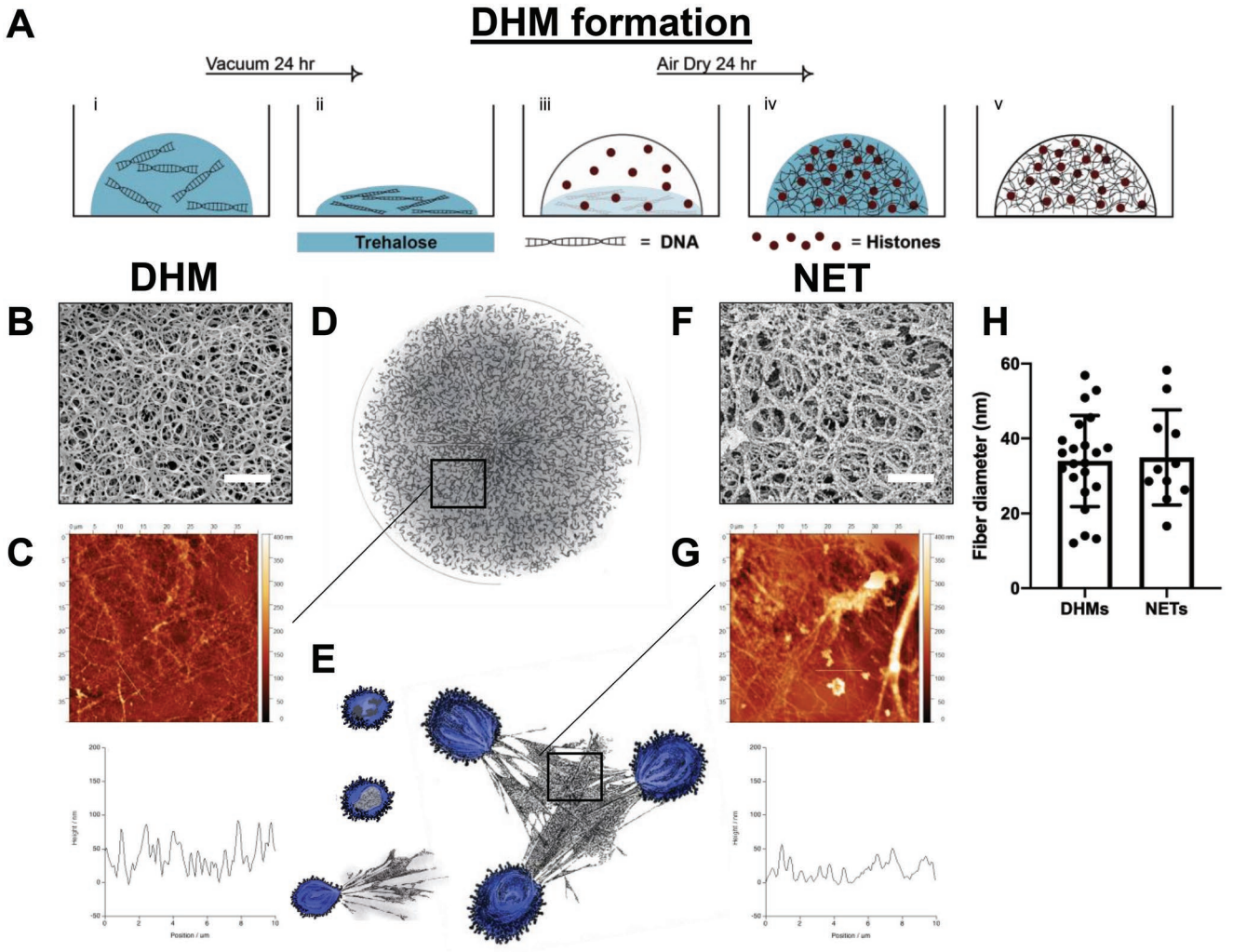

Figure 1. Formation and structural characterization of DHMs and their comparison to extracellular traps. A) i) DHMs are formed by the addition of a DNA-trehalose droplet to a well of a 96-well plate. ii) This droplet is dehydrated for 24 h under vacuum and iii) reconstituted with a histone solution. iv) Air drying the resulting structure for 24 h produces a vitrified shell, which can be rehydrated and washed away, v) leaving the pure structure attached to the 96-well plate bottom. B) SEM and C) AFM line profile scan of a DHM. D) An illustration of a sessile droplet-derived DHM structure, and its sequential dehydration-rehydration method of formation. E) An illustration of ET production showing the decondensing chromatin, and eventual ET release. F) SEM and G) AFM line profile scan of NET. H) Fiber diameters of DHMs and NETs were measured from on the SEM images. Scale bars = 20 µm.

(Figures S1, Supporting Information). Our optimized procedure involved the following steps. We first deposited 5–10 µL of methylated DNA (100 ng µL^{-1}; methylated 48 kbp lambda phage DNA) and trehalose (400 × 10^{-3} M) solution on a glass or polystyrene substrate and dehydrated for 24 h, yielding a vitrified shell structure. The inclusion of trehalose aided with the formation and stability of the final DHM, as trehalose is known to improve the uniformity of the dehydrated DNA layer[23–25] and stabilize both proteins[23] and nucleic acids[24] upon vitrification. Subsequent rehydration of the vitrified DNA-trehalose shell with 5–10 µL of a histone solution (2 mg mL^{-1}) formed a dense network of nanometer-scale fibers as evidenced by scanning electron microscopy (SEM) and atomic force microscopy (AFM) (Figure 1b–d). For comparison, endogenous neutrophil-derived ETs (NETs) exhibited similar morphology, size range, and fibrous pattern as shown by SEM, AFM, and immunohistochemistry (Figure 1e–g and Figure S2, Supporting Information), consistent with the literature.[7,26] In particular, analyses of the SEM images indicated comparable fiber diameters of DHMs and endogenous NETs, with the mean values of values of 33 ± 9 nm (DHMs) and 35 ± 13 nm (NETs) (Figure 1h). An additional 24 h re-vitrification of this network improved its structural integrity and substrate attachment, and a final rehydration and washing step removed all extraneous components and rendered the DHMs ready for use. These optimized procedures allow for the efficient patterning of large numbers of DHMs within multiwell plates ideal for high-throughput cell-based assays. Notably, a full 96-well plate with 8 µL DHM in each well requires only ≈77 µg DNA and 1.5 mg histones; an equivalent plate containing neutrophil-derived ETs could require in excess of 1 × 10^8 neutrophils.[22]

In order to interrogate the interaction of DHMs and immune cells, we added 10^4 murine bone marrow-derived dendritic cells (BMDCs) to 96-well plates containing DHMs or equivalent

© 2019 WILEY-VCH Verlag GmbH & Co. KGaA, Weinheim

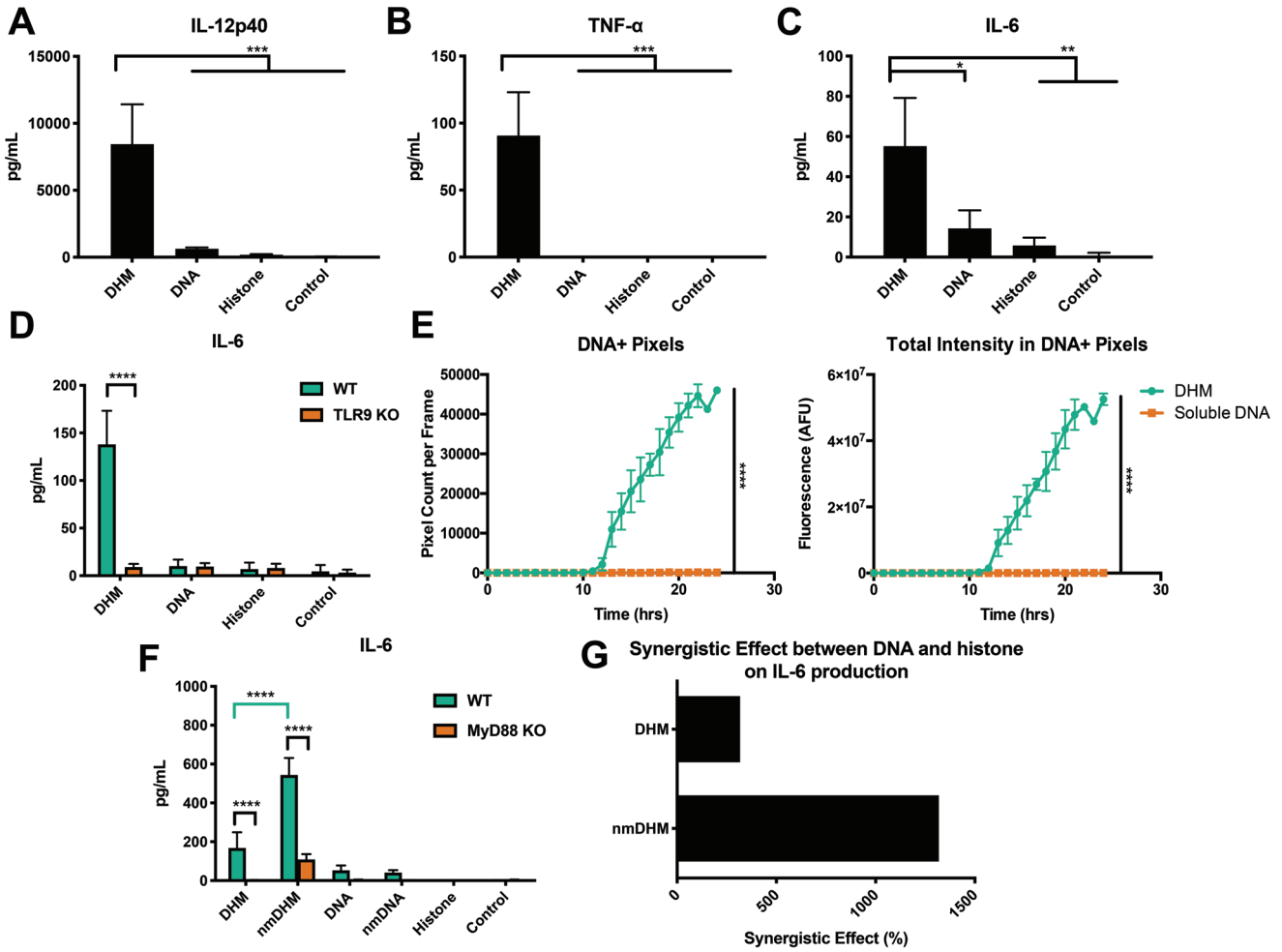

Figure 2. DHMs and nmDHMs induce inflammatory responses and promote DC uptake of DNA. BMDCs were incubated with DHMs or soluble component controls for 24 h, and supernatants were assayed by ELISA for A) IL-12p40, B) TNF-α, and C) IL-6. D) BMDCs from WT and TLR9$^{-/-}$ mice were incubated with DHMs or soluble controls for 24 h and assayed for IL-6 by ELISA. E) DCs were incubated with fluorophore-labeled DHMs or soluble DNA and monitored by live cell microscopy. DNA uptake by cells in fields of view proximal to DHMs or in soluble DNA-containing wells was quantified in both area (DNA + Pixels) and amount (total intensity in DNA + Pixels) F) WT or MyD88$^{-/-}$ mice were incubated with DHMs, nmDHMs, or soluble controls for 24 h. Supernatants were assayed for IL-6 by ELISA. G) Synergistic effect between DNA and histone was calculated for DHMs and nmDHMs using the data in (F). *$p < 0.05$, **$p < 0.01$, ***$p < 0.001$, and ****$p < 0.0001$.

mass of soluble DNA or histone controls for 24 h (**Figure 2**). DHMs triggered robust secretion of IL-12p40 from BMDCs, generating 13-fold and 48-fold higher levels of IL-12p40, compared with DNA and histone, respectively ($p < 0.001$, Figure 2a). Additionally, BMDCs incubated with DHMs produced TNF-α, whereas incubation with soluble DNA or histone did not produce any detectable levels of TNF-α ($p < 0.001$, Figure 2b). Last, DHMs improved secretion of IL-6 from BMDCs, with 3.8-fold ($p < 0.05$) and 9.6-fold ($p < 0.01$) increased levels, compared with DNA and histone, respectively (Figure 2c). DHM-mediated IL-6 production was dependent on Toll-like receptor-9 (TLR9), a DNA-sensing receptor in antigen-presenting cells;[27] DHM-triggered release of IL-6 was abrogated in BMDCs from TLR9$^{-/-}$ mice ($p < 0.0001$, Figure 2d). Additionally, this activation correlated with an increase in cellular uptake of the material, as cells proximal to fluorophore-labeled DHMs displayed significantly higher signal relative to dispersed soluble DNA in live cell microscopy (Figure 2e). Taken together, complexation of DNA and histones into ET-mimicking DHMs increases their cellular uptake and immunogenicity, demonstrating the immunostimulatory potential of the skeletal ET structure alone.

In addition to enabling the investigation of the DNA-histone backbone of ETs, DHMs provide a modular platform in which components can be exchanged or modified to study their individual roles in the ET structural framework. We leveraged this unique opportunity to examine the role of DNA methylation in ET-mediated immune activation. Endogenous ETs are composed of both methylated nuclear DNA and hypomethylated mitochondrial DNA;[10] while hypomethylated DNA is known to be immunostimulatory,[28,29] its specific and mechanistic contribution to ET immunogenicity remains unknown. We therefore used either methylated DNA or non-methylated DNA (nmDNA) to construct DHMs or nonmethylated DHMs (nmDHMs). BMDCs incubated with nmDHMs induced a 3.2-fold increase in IL-6 production, compared with the DHM group ($p < 0.0001$, Figure 2f). Intriguingly, soluble methylated

© 2019 WILEY-VCH Verlag GmbH & Co. KGaA, Weinheim

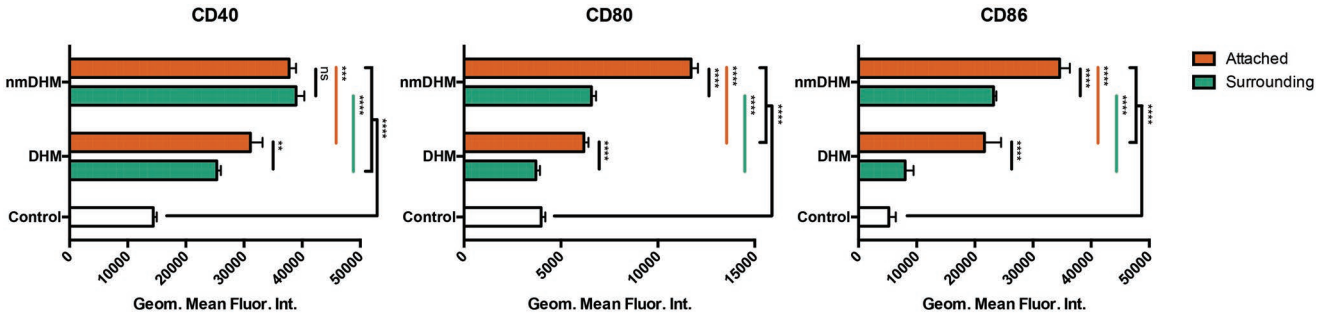

Figure 3. Contact-enhanced activation of DCs by DHMs. BMDCs were incubated with DHMs or nmDHMs for 18 h, after which DHMs/nmDHMs were removed from the well and digested with DNase I. Cells attached to and surrounding DHMs were analyzed for surface marker expression of CD40, CD80, and CD86 by flow cytometry. $^{**}p < 0.01$, $^{***}p < 0.001$, and $^{****}p < 0.0001$.

DNA and nmDNA both induced low levels of IL-6, suggesting amplified immune activation by nmDNA complexed into nmDHM. We also sought to ascertain whether immune activation by DHMs or nmDHMs was mediated by the MyD88 pathway downstream of TLR activation.[1] Upon incubation with either DHMs or nmDHMs, BMDCs from MyD88$^{-/-}$ mice produced significantly reduced levels of IL-6, compared with WT BMDCs ($p < 0.0001$, Figure 2f), indicating MyD88-mediated immune activation for both DHMs and nmDHMs. In addition, we calculated the "synergistic effect" between DNA and histone on DHM- or nmDHM-mediated production of IL-6, as shown in Equation (1)[30]

$$\text{Synergistic Effect} = \frac{\text{Effect of combinatorial stimulus}}{\sum(\text{Effect of individual stimuli})} \times 100\% \quad (1)$$

Compared with DHMs, nmDHMs exhibited a 4.2-fold increase in the synergistic effect (Figure 2g), suggesting that nonmethylated DNA amplifies the already synergistic nature of DNA-histone complexation shown in DHMs.

Due to the low yield of isolation procedures for endogenous ETs,[31] combined with the aforementioned heterogeneity of ET samples, it also remains challenging to study the role of physical interactions between immune cells and ETs. Our DHM platform permits such analysis, given its consistent and scalable nature. We leveraged this capacity to better understand how physical interaction of BMDCs with DHMs or nmDHMs impact DC activation. Specifically, after an 18 h BMDC-DHM co-culture, BMDCs physically adhered on DHMs, defined as "attached," were isolated by removing DHMs from wells via pipetting and digestion with DNase I. This cell fraction was then compared with the BMDCs which had adhered to the well bottom around the DHMs, defined as "surrounding" (Figure S3, Supporting Information). We then examined BMDCs for the expression of co-stimulation markers, CD40, CD80, and CD86 using flow cytometry. Consistent with cytokine data (Figure 2f), nmDHMs significantly enhanced the surface expression of CD40, CD80, and CD86 on BMDCs, compared with DHMs for BMDCs either "attached" to or "surrounding" the structures (**Figure 3**). Interestingly, all markers of DC activation, with the exception of CD40 for nmDHMs, were significantly increased on "attached" BMDCs compared with "surrounding" cells, suggesting the importance of physical contact in promoting immune activation. Taken together, these results show that physical contact between DCs and DHMs/nmDHMs induces robust immune response.

In summary, we have developed DHMs mimicking the skeletal DNA-histone substructure of ETs and demonstrated their pro-inflammatory nature. We have shown that DNA and histone formulated into DHMs promote synergistic activation of DCs, dependent on classic TLR signaling pathways, and that immune activation is further amplified by the inclusion of nmDNA in DHMs. Additionally, our studies provide preliminary evidence for the importance of physical contact between DNA-histone fibers and DCs in prompting an immunostimulatory response. These findings shed light on the established immune activation mediated by ETs, indicating that such behavior can be at least partly attributed to the complexed DNA-histone backbone. The spatiotemporal proximity of DNA and histones complexed together in this manner mediates a potent immunogenic combination upon which other ET components can build.

More broadly, our DHM platform represents an opportunity to study the ET substructure and its role in other pathophysiological conditions. As described in this report, its modularity allows for the insertion or swapping of individual components, which will enable investigations on the effects of individual ET-associated proteins and peptides. The combination of clinical promise and interest in ETs alongside the aforementioned challenges of mechanistically studying biological samples in vitro position this platform to shed further insight on the diverse physiological and pathophysiological impact of ETs.

Experimental Section

Formation of DHMs: Methylated (Item No. 91080-14-7, Millipore Sigma, Burlington, MA, USA) and nonmethylated (Item No N3011, New England Biolabs, Ipswich, MA, USA) lambda-phage DNA, and α,α-trehalose dihydrate (Item No T-104-4, Pfansteihl Inc, Waukegan, IL, USA) were solubilized in ultrapure water and combined to a final concentrations of 100 ng μL^{-1} and 400×10^{-3} M, respectively. Droplets of 5–10 µL DNA-trehalose solution were dispensed into 96-well plate wells and dehydrated in a desiccator for ≈24 h at 20 mmHg. The vitrified DNA-trehalose deposit was then rehydrated with an equivalent volume of 2 mg mL^{-1} calf thymus histone (Item No 9064-47-5, Millipore Sigma, Burlington, MA, USA) in 10×10^{-3} M Tris-HCl. These structures were dehydrated for ≈24 h at room temperature/pressure. Prior to their use, DHMs were washed with 100 µL changes of 10×10^{-3} M Tris-HCl.

© 2019 WILEY-VCH Verlag GmbH & Co. KGaA, Weinheim

AFM Imaging: 10 µL DHMs were prepared in each well of an 8-well chambered coverslip (Item No 80826, ibidi GmbH, Martinsried, Germany), washed, and fixed using 4% PFA/PBS overnight. For primary cell-derived NETs, neutrophils were isolated from a single 30 mL human whole blood sample using the commercially available MACSxpress Neutrophil Isolation Kit (Item No 130-104-434, Miltenyi Biotec GmbH, Bergisch Gladbach, Germany), yielding ≈19.6×10^6 cells that were suspended in RPMI culture media supplemented with 3% FBS and 1% anti–anti. A 150 µL volume solution containing 100 µL of cell suspension (10^6 cells mL^{-1}) and 50 µL of additional culture media was added to each well of an 8-well chambered coverslip (Item No 80826, ibidi GmbH). NETosis was induced by adding 50 µL of 400×10^{-9} M PMA (to a final concentration of 100×10^{-9} M PMA) to each well and incubating neutrophils for ≈4 h to allow for the formation of NETs. The resulting NETs were then gently washed using PBS and fixed using 4% PFA/PBS overnight. Fixed NETs and DHMs were washed with DI-water and dried in a desiccator overnight. Chambered side walls were detached prior to imaging. AFM imaging was performed using a scanning probe microscope (Model Dimension 3100, Veeco Instruments, Inc., Plainview, New York, USA) using a pyramidal Si tip (Item No ACST-10, Applied NanoStructures, Inc., Mountain View, CA, USA). Resulting data was analyzed using the open-source Gwyddion SPM analytical software (Český Metrologický Institut, Brno, Czech Republic).

SEM Imaging: 8 µL DHMs and ETs were fixed overnight in 2% PFA/PBS (Item No 15735, Electron Microscopy Services, Hatfield, PA, USA). Samples were washed with DI water, incubated overnight in 1% osmium tetroxide (Item No 19140, Electron Microscopy Sciences), washed using DI water, and subjected to ethanol dehydration across 10%, 25%, 50%, 75%, 95%, and 100% ethanol (Item No 64-17-5, Thermo Fisher Scientific, Waltham, MA, USA) solutions at 10–15 min per solution. Samples were then washed twice with hexamethyldisilazane (Item No 16700, Electron Microscopy Sciences), which was evaporated at room temperature overnight, coated with gold using a modular sputter coater (SPI Supplies, West Chester, PA, USA), and imaged using a SEM/FIB (Model NOVA 200 NanoLab, FEI Company, Hillsboro, OR, USA).

DHM Fluorescent Microscopy: 10 µL DHMs were prepared as previously described in each well of an 8-well chambered coverslip (Item No 80826, ibidi GmbH), washed, and immersed in 200 µL of PBS containing 3% BSA. DNA present within DHMs was labeled using 0.1% (v/v) DAPI (Item No D1306, ThermoFisher Scientific), 0.01% (v/v) Sytox Green (Item No S7020, ThermoFisher Scientific), or 0.001% (v/v) PicoGreen (Item No P7581, ThermoFisher Scientific); and histones were immuno-labeled for 3 h using 1 µg mL^{-1} anti-H1 (Item No ab4629, Abcam, Cambridge, UK), -H2B (Item No ab1790, Abcam), -H3 (Item No ab1791, Abcam), or -H4 (Item No ab31830, Abcam) primary mAbs (1 µg per 5 µg DNA) derived from mouse or rabbit. The pre-stained DHMs were washed with PBS containing 1% BSA and incubated with 1 µg mL^{-1} Alexa 568- or 647-labeled donkey-anti-mouse (Item No 20802, Biotium Inc., Fremont, CA, USA) and donkey-anti-rabbit (Item No 20811, Biotium Inc.) mAbs, respectively for 3 h. The final immunostained DHMs were washed with PBS three times and imaged by a spinning disk confocal microscope (Model UltraVIEW VoX, PerkinElmer, Inc., Waltham, MA, USA). The final multilayered images were generated and analyzed using the open-source ImageJ software (NIH).

BMDC Isolation and Culture: All work performed on animals was in accordance with and approved by the University Committee on Use and Care of Animals (UCUCA) at the University of Michigan, Ann Arbor (#PRO00008587). BMDCs were prepared as previously reported.[32] Briefly, murine femurs and tibiae were isolated from 6–8-week-old female C57BL/6 mice (Jackson Laboratory), BALB/c mice (Envigo), or $TLR9^{-/-}$ or $MyD88^{-/-}$ mice and flushed to extract the bone marrow. After dispersal of aggregates, cells were plated in GM-CSF-containing RPMI (Item No 11875093, ThermoFisher Scientific) in Petri dishes and cultured for 10–12 days.

BMDC/DHM Analysis: For cytokine measurements, 10^4 BMDCs were seeded in 96-well plates containing DHMs or controls. After 24 h incubation, supernatants were collected and immediately frozen for later ELISA analysis (Item Nos DY 406/DY 410/DY 499, DuoSets, R&D Systems, Minneapolis, MN, USA). For flow cytometry, 2.5×10^4 BMDCs per well were added to 96-well plates wherein 36 wells contained DHMs and 24 wells were blank controls. For each replicate, the 36 DHMs were forcefully pipetted into a separate container and centrifuged, after which the supernatant was removed and replaced with 10 U mL^{-1} DNase I (Item No D5025, Millipore Sigma) in a Ca^{2+} and Mg^{2+}-supplemented 10×10^{-3} M Tris-HCl buffer. In parallel, cells remaining in the DHM-containing and control wells were detached (using trypsin) and treated with DNase I. Cells were then washed; blocked with an anti-CD16/32 antibody (clone 93, Item No 50-112-9520, eBioscience); treated with antibodies directed against CD40 (clone 3/23, Item No 745218, Becton Dickinson), CD80 (clone 1G10, Item No A14724, Invitrogen), and CD86 (clone GL1, Item No 560582, Becton Dickinson); and analyzed by flow cytometry.

DNA was pre-labeled with Label IT commercial labeling kit (Mirus Bio), formed into DHMs as previously described or left in soluble form, and added to 12 well plates. BMDCs were plated at 500 000 cells/well and imaged using a fully-motorized inverted microscope (Olympus) affixed with a humidified isolation chamber maintained at 37 °C and 5% CO_2. Time series images were acquired at fixed coordinates proximal to the DHM or in the soluble DNA wells over 24 hours, after which they were validated to confirm proper operation of autofocus machinery; image stacks which did not indicate reliable autofocus across the time series were removed from the data set. The remaining image frames, n = 2 for DHM and n = 7 for soluble DNA, were compiled with ImageJ software (NIH) analyzed using an in-house MATLAB script to quantify DNA uptake and retention.

Statistical Analyses: Statistics were acquired with GraphPad Prism 6.0 (GraphPad) using one- or two-way ANOVA tests with Tukey's multiple comparisons correction. Values are reported as mean ± SD with the following statistical values: $*p < 0.05$, $**p < 0.01$, $***p < 0.001$, and $****p < 0.0001$.

Supporting Information

Supporting Information is available from the Wiley Online Library or from the author.

Acknowledgements

P.D.W., C.L., and T.K. contributed equally to this work. This work was supported in part by NIH (R01EB022563, R01AI127070, R01CA210273, R01CA223804, U01CA210152, R01GM123517, and R01HL136141). J.J.M. is a Young Investigator supported by DoD/CDMRP Peer Reviewed Cancer Research Program (W81XWH-16-1-0369) and NSF CAREER Award (1553831). Opinions interpretations, conclusions, and recommendations are those of the author and are not necessarily endorsed by the Department of Defense. C.L. is supported by a predoctoral fellowship from the Cellular Biotechnology Training Program (T32GM008353) and a Graduate Assistance in Areas of National Need Fellowship awarded to the University of Michigan. The authors wish to thank Dr. Beth Moore, Giovanny Martinez-Colon, Dr. Gabriel Núñez, and Caitlin Reynolds for providing knockout tissues; Dr. Joel Whitfield and the Immunology Core at the University of Michigan Cancer Center for performing all ELISA analyses, and Glenn Walker (Eastern Michigan University), Ahmet Emrehan, and the University of Michigan MC^2 technical staff for assisting with sample preparation and acquisition of SEM images. In addition, the authors wish to express their gratitude to Drs. Theodore Standiford, Gabriel Núñez, Joel Whitfield, and Nilay Chakraborty for thoughtful conversations and insights that proved invaluable for planning experiments and interpreting the data presented herein.

Conflict of Interest

The authors declare no conflict of interest.

© 2019 WILEY-VCH Verlag GmbH & Co. KGaA, Weinheim

Keywords

DNA, extracellular traps, histones, immunostimulation, methylation

Received: July 15, 2019
Revised: September 13, 2019
Published online: October 15, 2019

[1] C. J. Desmet, K. J. Ishii, *Nat. Rev. Immunol.* **2012**, *12*, 479.
[2] R. Barbalat, S. E. Ewald, M. L. Mouchess, G. M. Barton, *Annu. Rev. Immunol.* **2011**, *29*, 185.
[3] J. Wu, Z. J. Chen, *Annu. Rev. Immunol.* **2014**, *32*, 461.
[4] K. Yasuda, P. Yu, C. J. Kirschning, B. Schlatter, F. Schmitz, A. Heit, S. Bauer, H. Hochrein, H. Wagner, *J. Immunol.* **2005**, *174*, 6129.
[5] R. Lande, J. Gregorio, V. Facchinetti, B. Chatterjee, Y.-H. Wang, B. Homey, W. Cao, Y.-H. Wang, B. Su, F. O. Nestle, T. Zal, I. Mellman, J.-M. Schröder, Y.-J. Liu, M. Gilliet, *Nature* **2007**, *449*, 564.
[6] J. Tian, A. M. Avalos, S.-Y. Mao, B. Chen, K. Senthil, H. Wu, P. Parroche, S. Drabic, D. Golenbock, C. Sirois, J. Hua, L. L. An, L. Audoly, G. La Rosa, A. Bierhaus, P. Naworth, A. Marshak-Rothstein, M. K. Crow, K. A. Fitzgerald, E. Latz, P. A. Kiener, A. J. Coyle, *Nat. Immunol.* **2007**, *8*, 487.
[7] V. Brinkmann, *Science* **2004**, *303*, 1532.
[8] B. McDonald, R. Urrutia, B. G. Yipp, C. N. Jenne, P. Kubes, *Cell Host Microbe* **2012**, *12*, 324.
[9] G. Papadaki, K. Kambas, C. Choulaki, K. Vlachou, E. Drakos, G. Bertsias, K. Ritis, D. T. Boumpas, P. R. Thompson, P. Verginis, P. Sidiropoulos, *Eur. J. Immunol.* **2016**, *46*, 2542.
[10] C. Lood, L. P. Blanco, M. M. Purmalek, C. Carmona-Rivera, S. S. De Ravin, C. K. Smith, H. L. Malech, J. A. Ledbetter, K. B. Elkon, M. J. Kaplan, *Nat. Med.* **2016**, *22*, 146.
[11] R. Khandpur, C. Carmona-Rivera, A. Vivekanandan-Giri, A. Gizinski, S. Yalavarthi, J. S. Knight, S. Friday, S. Li, R. M. Patel, V. Subramanian, P. Thompson, P. Chen, D. A. Fox, S. Pennathur, M. J. Kaplan, *Sci. Transl. Med.* **2013**, *5*, 178ra40.
[12] K. Kessenbrock, M. Krumbholz, U. Schönermarck, W. Back, W. L. Gross, Z. Werb, H.-J. Gröne, V. Brinkmann, D. E. Jenne, *Nat. Med.* **2009**, *15*, 623.
[13] S. Sangaletti, C. Tripodo, C. Chiodoni, C. Guarnotta, B. Cappetti, P. Casalini, S. Piconese, M. Parenza, C. Guiducci, C. Vitali, M. P. Colombo, *Blood* **2012**, *120*, 3007.
[14] R. Lande, D. Ganguly, V. Facchinetti, L. Frasca, C. Conrad, J. Gregorio, S. Meller, G. Chamilos, R. Sebasigari, V. Riccieri, R. Bassett, H. Amuro, S. Fukuhara, T. Ito, Y.-J. Liu, M. Gilliet, *Sci. Transl. Med.* **2011**, *3*, 73ra19.
[15] E. Villanueva, S. Yalavarthi, C. C. Berthier, J. B. Hodgin, R. Khandpur, A. M. Lin, C. J. Rubin, W. Zhao, S. H. Olsen, M. Klinker, D. Shealy, M. F. Denny, J. Plumas, L. Chaperot, M. Kretzler, A. T. Bruce, M. J. Kaplan, *J. Immunol.* **2011**, *187*, 538.
[16] S. Yousefi, J. A. Gold, N. Andina, J. J. Lee, A. M. Kelly, E. Kozlowski, I. Schmid, A. Straumann, J. Reichenbach, G. J. Gleich, H.-U. Simon, *Nat. Med.* **2008**, *14*, 949.
[17] S. Yousefi, C. Mihalache, E. Kozlowski, I. Schmid, H. U. Simon, *Cell Death Differ.* **2009**, *16*, 1438.
[18] J. Xu, X. Zhang, M. Monestier, N. L. Esmon, C. T. Esmon, *J. Immunol.* **2011**, *187*, 2626.
[19] C. F. Urban, D. Ermert, M. Schmid, U. Abu-Abed, C. Goosmann, W. Nacken, V. Brinkmann, P. R. Jungblut, A. Zychlinsky, *PLoS Pathog.* **2009**, *5*, e1000639.
[20] Y. Nishikawa, Y. Kajiura, J. H. Lew, J. I. Kido, T. Nagata, K. Naruishi, *J. Cell. Physiol.* **2017**, *232*, 1862.
[21] C. H. Lim, S. S. Adav, S. K. Sze, Y. K. Choong, R. Saravanan, A. Schmidtchen, *Front. Immunol.* **2018**, *9*, 1554.
[22] S. Najmeh, J. Cools-Lartigue, B. Giannias, J. Spicer, L. E. Ferri, *J. Visualized Exp.* **2015**, *98*, e52687.
[23] N. K. Jain, I. Roy, *Protein Sci.* **2009**, *18*, 24.
[24] J. Bonnet, M. Colotte, D. Coudy, V. Couallier, J. Portier, B. Morin, S. Tuffet, *Nucleic Acids Res.* **2010**, *38*, 1531.
[25] D. R. Adams, M. Toner, R. Langer, *Langmuir* **2008**, *24*, 7688.
[26] R. H. Pires, S. B. Felix, M. Delcea, *Nanoscale* **2016**, *8*, 14193.
[27] K. Takeda, S. Akira, *Semin. Immunol.* **2004**, *16*, 3.
[28] L. V. Collins, S. Hajizadeh, E. Holme, I. M. Jonsson, A. Tarkowski, *J. Leukocyte Biol.* **2004**, *75*, 995.
[29] B. Liu, Q. Du, L. Chen, G. Fu, S. Li, L. Fu, X. Zhang, C. Ma, C. Bin, *Sci. Rep.* **2016**, *6*, 23421.
[30] M. Krummen, S. Balkow, L. Shen, S. Heinz, C. Loquai, H. C. Probst, S. Grabbe, *J. Leukocyte Biol.* **2010**, *88*, 189.
[31] V. Brinkmann, B. Laube, U. Abu Abed, C. Goosmann, A. Zychlinsky, *J. Visualized Exp.* **2010**, *36*, e1724.
[32] M. B. Lutz, N. Kukutsch, A. L. Ogilvie, S. Rossner, F. Koch, N. Romani, G. Schuler, *J. Immunol. Methods* **1999**, *223*, 77.

© 2019 WILEY-VCH Verlag GmbH & Co. KGaA, Weinheim